Charge-State Distribution and Doppler Effect in an Expanding Photoionized Plasma

M. E. Foord,[1] R. F. Heeter,[1] P. A. M. van Hoof,[2] R. S. Thoe,[1] J. E. Bailey,[3] M. E. Cuneo,[3] H.-K. Chung,[1] D. A. Liedahl,[1] K. B. Fournier,[1] G. A. Chandler,[3] V. Jonauskas,[2] R. Kisielius,[2] L. P. Mix,[3] C. Ramsbottom,[2] P. T. Springer,[1] F. P. Keenan,[2] S. J. Rose,[4] and W. H. Goldstein[1]

[1]*Lawrence Livermore National Laboratory, University of California, Livermore, California 94551, USA*
[2]*APS Division, Physics Department, Queen's University Belfast, Belfast BT7 1NN, Northern Ireland, United Kingdom*
[3]*Sandia National Laboratory, Albuquerque, New Mexico, 37185, USA*
[4]*Dept. of Physics, Clarendon Laboratory, Oxford OX1 3PU, United Kingdom*

(Received 24 February 2004; published 29 July 2004)

The charge state distributions of Fe, Na, and F are determined in a photoionized laboratory plasma using high resolution x-ray spectroscopy. Independent measurements of the density and radiation flux indicate unprecedented values for the ionization parameter $\xi = 20$–25 erg cm s^{-1} under near steady-state conditions. Line opacities are well fitted by a curve-of-growth analysis which includes the effects of velocity gradients in a one-dimensional expanding plasma. First comparisons of the measured charge state distributions with x-ray photoionization models show reasonable agreement.

DOI: 10.1103/PhysRevLett.93.055002 PACS numbers: 52.50.Jm, 52.25.Kn

With the recent launch of the x-ray observatories Chandra and XMM-Newton, high resolution spectral data from numerous astrophysical x-ray sources such as accretion-driven binary systems and active galactic nuclei have been reported [1,2]. Discrete emission and absorption spectra from such objects are extremely complex. Interpreting such spectra requires detailed modeling of the radiation field and its interactions with the free and bound electrons, including the most accurate atomic data available. Laboratory studies, using, for example, electron-beam ion traps [3], storage rings [4], and tokamaks [5] have provided atomic data that have been incorporated into astrophysical spectral synthesis codes. However, until recently [6–10], creating an appropriate x-ray environment to carry out well characterized photoionization experiments under near steady-state conditions has not been possible, owing to the lack of a high fluence x-ray source. In this Letter, we present results from our Z-pinch experiments, where the x-ray emission from the pinch photoionizes Fe into the L shell and Na and F into the K shell. Using high resolution x-ray spectroscopy and other x-ray diagnostics, the charge state distribution, the absolute radiative flux, and the sample densities are measured independently. These allow the first direct comparisons with photoionization models in the relatively low density ($n_e = 2 \times 10^{19}$ cm^{-3}) two-body recombination regime.

These experiments were performed at the Sandia National Laboratory Z facility. The radiation from the pinch is generated by coupling a 20 MA, 100 ns rise time current pulse into a 2 cm diameter, 1 cm length, cylindrical wire array. The electromagnetic forces drive the 11.5 μm diameter tungsten wires radially inward onto the central axis, creating a 8 ns FWHM, 120 TW, 165 eV near-blackbody radiation source. An absolutely calibrated transmission grating spectrometer measures the spectral and temporal emission from the pinch [11] (see Fig. 1). The pinch emission provides a sufficient x-ray flux to photoionize iron into the L shell and also produces a relatively line-free quasicontinuum source of x rays in the 9–17 Å wavelength range as needed for the absorption experiments described below [6,8–10]. Also shown in Fig. 1 are comparisons with filtered x-ray detectors (XRDs) [12] which show reasonable agreement over most of the energy range. Above 2 keV, spectra were measured using filtered photoconducting detectors (PCDs) [13]. The results presented below were found to be relatively insensitive to the small high energy component above 2 keV.

Thin rectangular foils were suspended in frames and positioned 1.5–1.6 cm from the z axis of the pinch. The foils consisted of 500–750 Å thick, 1.35:1 molar ratio of Fe/NaF and were overcoated on each side with 1000 Å of

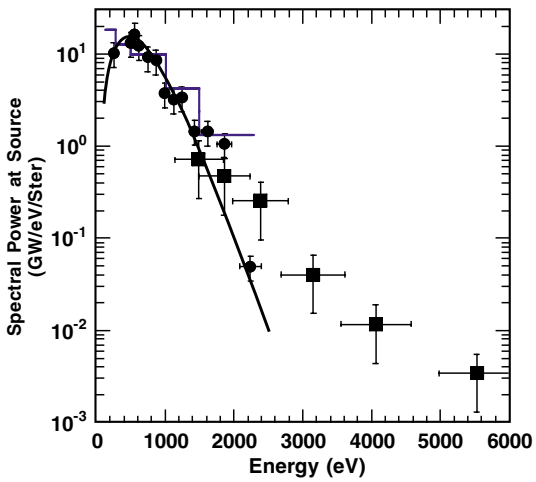

FIG. 1 (color online). Z-pinch x-ray spectral emission measured at peak power with an XRD array (stepped lines), a transmission grating spectrometer (dots), and a PCD array (squares). Shown for comparison is a peak-normalized 165 eV blackbody spectrum.

lexan $(C_{16}H_{14}O_3)_n$ to help maintain uniform conditions during heating and expansion. During the initial 100 ns run-in phase, radiation from the wires preheated the foils, and the central Fe/NaF portion of the foil typically expanded 1.5–2 mm, decreasing the density by many orders of magnitude. A time-gated filtered x-ray pinhole camera imaged the Fe/NaF emission region edge-on, thus determining the time history of the average density. When the wires collide on axis, the resulting x-ray pulse quickly photoionizes the low density expanded foil.

At sufficiently low density where two-body processes dominate, the degree of ionization can be shown to mainly depend on the ionization parameter $\xi \equiv 16\pi^2 J/n_e$ [14], where J is the mean intensity, $J \equiv (1/4\pi) \iint J_\nu(\Omega) d\Omega d\nu$ integrated over solid angle and integrated in energy from $\chi_H = 13.6$ eV to infinity. ξ is a scaling parameter used in astrophysics for determining the ionization state in photoionized plasma. Here ξ reaches a value near 25 $\mathrm{erg\,cm\,s^{-1}}$ at the peak of the radiation pulse.

Quasicontinuum x-ray radiation produced by the pinch is absorbed as it passes through the photoionized plasma and is recorded on film using a time-integrated convex potassium hydrogen phthalate crystal spectrometer. Over the 8.5–17 Å wavelength range the instrumental resolution was $E/\Delta E \simeq 500$–800. Typical absorption data over the 8.5–12 Å portion of the spectrum are shown in Fig. 2, where K-shell absorption lines for Na and F ions, and L-shell absorption lines for iron are observed.

The Na and F absorption lines were analyzed using a simple one-dimensional expansion model. Hydrodynamic simulations indicate that during the initial heating and expansion phase, the central Fe/NaF portion of the foil remains fairly uniform due to the tamping effect of the lexan overcoat. The velocity profile is well approximated by the linear self-similar form $u(x) = u_0(x/x_0)$, where u_0 and x_0 are the velocity and position at the edge, relative to the foil center. The optical depth for a photon passing normal through this expanding one-dimensional plasma is given by

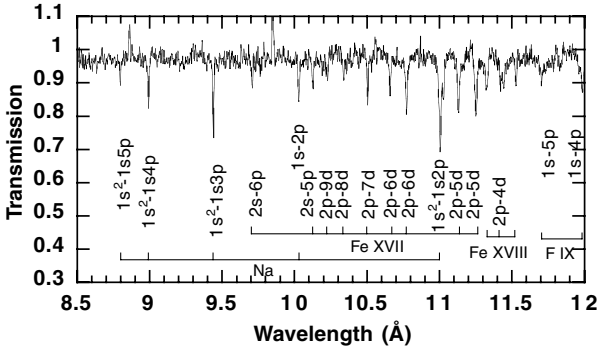

FIG. 2. Absorption spectrum of L-shell iron and K-shell sodium and fluorine lines. Unidentified peaks at 8.8 and 9.8 Å are due to film defects.

$$\tau_\nu = \int_{-u_0}^{u_0} du \frac{k_0}{\sqrt{\pi} u_0 \sigma} \exp\left\{\frac{-[\nu\{1 - u(x)/c\} - \nu_0]^2}{\sigma^2}\right\}, \tag{1}$$

where σ is the transition linewidth. $1 - u(x)/c$ is the Doppler factor due to expansion, and $k_0 \equiv \pi e^2 f_{\mathrm{osc}} N_i L / 2mc$, which depends on the oscillator strength of the line transition. Here $L \equiv 2x_0$ and $N_i L$ is the areal density of the ground state configuration for ion i. Line shapes are dominated by Doppler broadening effects, except for the case of Na He-δ, where Stark broadening increases the linewidth by $\approx 5\%$ at $T_i = 150$ eV. Stimulated emission is small and not included. Because the expansion is approximately one dimensional and the ground-state populations dominate the total population of each ion stage, the areal density can be written as $\sum_i N_i L = N_o L_o$, where $N_o L_o$ is the initial areal density of the solid foil (provided by the manufacturer). Thus, $N_i L = f_i N_o L_o$, where f_i is the fractional charge state abundance of ion i.

Defining the new variables $y = (\nu - \nu_0)/\sigma$ and $w = y - u/u_{\mathrm{th}}$, using $u_{\mathrm{th}} = \sigma c/\nu_0$ and $u/c \ll 1$, and assuming that the sample density is approximately uniform, the optical depth is rewritten as

$$\begin{aligned}\tau_\nu &= \frac{k_0 u_{\mathrm{th}}}{\sigma u_0} \int_{y - u_0/u_{\mathrm{th}}}^{y + u_0/u_{\mathrm{th}}} \frac{e^{-w^2}}{\sqrt{\pi}} dw \\ &= \frac{k_0}{2\sigma} \frac{\{\mathrm{erf}(y + u_0/u_{\mathrm{th}}) - \mathrm{erf}(y - u_0/u_{\mathrm{th}})\}}{u_0/u_{\mathrm{th}}}. \end{aligned} \tag{2}$$

This expression reduces to a Gaussian profile having a thermal width σ for the stationary case where $u_0/u_{\mathrm{th}} \ll 1$ and approaches a rectangular function for the case $u_0/u_{\mathrm{th}} \gg 1$.

The instrumental resolution of the crystal spectrometer was insufficient to resolve the line profiles in these relatively low temperature plasmas. However, the spectrally integrated line strength is independent of the instrumental resolution. Hence we define the measured line absorption strength (equivalent width) as $A = \int\{1 - \exp(-\tau_\nu)\} d\nu$, where τ_ν is given in Eq. (2). This yields a "curve of growth" relationship, often applied in interpreting astrophysical line strengths [15]

$$\frac{A}{\sigma} = \int\{1 - \exp(-\tau_\nu)\} dy = \int[1 - \exp\{-\tau_0 g(y)\}] dy, \tag{3}$$

where $\tau_0 = 2k_0/\sqrt{\pi}\sigma$ is the unshifted line-center optical depth and $g(y)$ is defined through Eq. (2). For optically thin lines where $\tau_0 < 1$, Eq. (3) predicts that the ratio of A/σ is approximately proportional to τ_0. In the optically thick regime, A/σ depends on both τ_0 and u_0/u_{th} since the center of the line starts to saturate. The transition from an optically thin linear regime to an optically thick nonlinear regime at larger τ_0 is evident in Fig. 3. By fitting a range of data from relatively weak to strong

absorption lines, the relative concentrations of each ion, f_i, can be determined.

The analysis is applied to the Na and F absorption spectrum shown in Fig. 2. The absorption strengths of the Na lines $1s^2 - 1s2p$, $1s^2 - 1s3p$, $1s^2 - 1s4p$, $1s^2 - 1s5p$, and the $1s - 2p_{1/2,3/2}$ doublet were determined by numerical integration across each respective absorption line. The absorption lines are mainly broadened by thermal effects and from the expansion of the plasma. As discussed below, the electron temperature is estimated to be approximately 150 eV. At these conditions, the temperature equilibration time between Fe^{16+} ions and electrons is approximately 1 ns [16]. Therefore, here we assume $T_i = 150$ eV as well. Shown in Fig. 3 is a calculation with $T_i = 150$ eV and $u_0/u_{\rm th} = 0.83$. The data are well fitted by this distribution over a wide range of line strengths. The resulting ratio of Na^{10+}:Na^{9+} (H-like:He-like) ground state ions is 1:4.5. Note that the determination of the ionization balance depends mostly on the relative absorption strengths of lines from each ion stage and is relatively insensitive to the ion temperature. A similar analysis of F absorption lines indicates a ratio of 6.0:1 for F^{8+}:F^{7+}. The reversed ratio for F relative to Na is due to its lower photoionization threshold.

The Fe absorption spectrum was analyzed using the one-dimensional expansion model described above. Line positions and oscillator strengths for many thousands of Fe lines were calculated using the HULLAC suite of codes [17]. In cases where nearby lines were strongly blended, more accurate line positions from Kelly [18] were used. The charge state distribution was then determined by varying each iron charge state concentration, f_i, to best fit the absorption line strengths. The resulting charge state distribution for Fe is shown in Fig. 4. Uncertainties in the background level and signal to noise of the absorption spectrum were used to estimate the uncertainties in the charge state populations for each ion. The average charge state for Fe is $\langle Z \rangle = 16.1 \pm 0.2$.

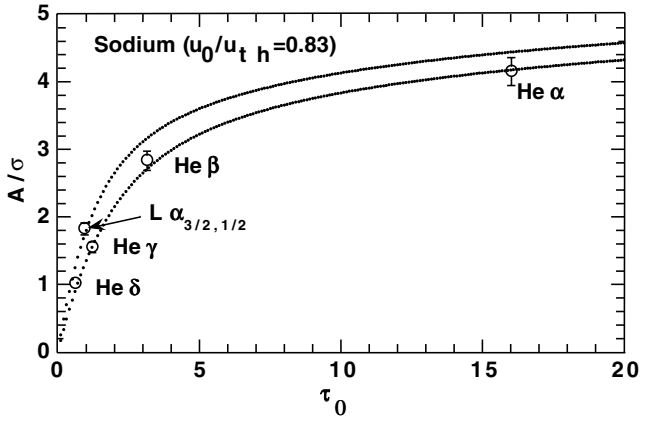

FIG. 3. Curve-of-growth analysis for sodium absorption lines. Vertical error bars assume ±5% uncertainty in the absorption strength for each line. The upper curve was calculated for the blended Lyα(3/2,1/2) lines separated by 6 mÅ.

The charge state distributions for Fe, Na, and F were calculated with the collisional-radiative code GALAXY [19]. For a given density, temperature, and incident radiation field, GALAXY calculates the steady-state ionization balance within the plasma. Collisional and radiative excitation and ionization as well as autoionization and all reverse processes are included. Hartree-Dirac-Slater (HDS) cross sections are used for photoionization. The GALAXY code employs an average-of-configuration approximation for electronic states with a principal quantum number $n \leq 5$ and configuration averages for higher n.

In order to account for the estimated few ns required to reach steady-state equilibrium [20], the values of the absolute spectral flux and sample density ($n_e = 2.0 \pm 0.7 \times 10^{19}$ cm^{-3}) used in the calculations were taken at +3 ns after the peak of the radiation pulse. We estimate that ξ decreases from 25 to 20 erg cm s^{-1} during this time, which has a very small effect on the ionization balance. At this density, the charge state distribution for Fe was calculated for various temperatures between 30 and 210 eV (see Fig. 4). Above 70 eV, the distributions peak near Fe^{16+} and are quite insensitive to the electron temperature. In this temperature regime (90 to 210 eV) calculations indicate that photoionization of Fe L-shell ions dominates over collisional ionization processes by more than a factor of 10. The weak temperature dependence of the charge state distribution therefore is likely due to the thermal electrons having insufficient energy to ionize the L-shell ions in this regime. Below 50 eV, the contribution from three-body recombination begins to dominate, reducing the degree of ionization substantially.

The average charge state predicted by GALAXY in the 90 to 210 eV temperature range is $\langle Z \rangle \simeq 16.4 \pm 0.2$ (see

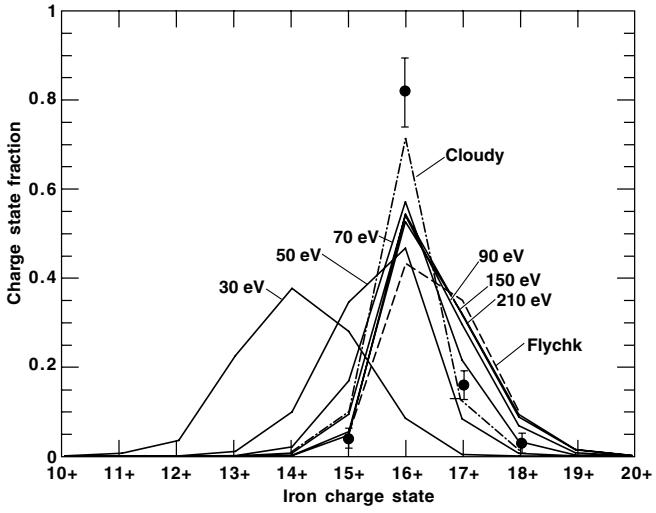

FIG. 4. Iron charge state distribution (solid dots) and comparisons with photoionization code GALAXY for $T_e =$ 30–210 eV (solid lines). Also shown are results from the code FLYCHK at $T_e = 150$ eV (dashed line) and CLOUDY (dash-dotted line).

Fig. 4). The uncertainty in $\langle Z \rangle$ is determined from folding in the sensitivities to the uncertainties in the absolute flux ($\pm 20\%$) and density ($\pm 35\%$) measurements. The calculated distribution is slightly more ionized than measured. This may be due, in part, to the fact that the measured time-integrated absorption spectrum is weighted by the time history of the backlighter intensity, which peaks a few ns before the sample reaches steady-state equilibrium, resulting in a slightly lower average charge. GALAXY calculations of H- to He-like ratios for F and Na yielded ratios of 6.7:1 and 1:1.4, respectively, at $T_e = 150$ eV. The F ratio agrees well with the data (6.0:1), while the Na data (1:4.5) is substantially less ionized than predicted.

For comparison, the photoionization code CLOUDY [21] was also employed. CLOUDY generally uses simpler atomic modeling than GALAXY but incorporates better atomic data and can also calculate the electron temperature independently. CLOUDY calculates the temperature by a detailed energy accounting of all relevant heating and cooling processes, such as collisional excitation followed by radiative cooling. Our first model calculation included a restricted set of Fe emission lines that effectively treated the Fe resonance lines as optically thick. This assumption is consistent with the measured saturation of the strongest Fe lines and the curve of growth plots shown in Fig. 3. This model yielded an electron temperature near $T_e = 150$ eV and an average charge state $\langle Z \rangle \simeq 16.0$, in reasonable agreement with both the measured distribution width and the average ionization state (see Fig. 4). To test the sensitivity to optical depth effects, a second model was constructed which treated all lines as optically thin. This optically thin model yielded a much lower temperature $T_e = 38$ eV, due to enhanced cooling from line emission, and a distribution that peaked at Fe^{12+}. The optically thin approximation is therefore inconsistent with our data but does set a lower limit on the temperature due to line transport.

Also shown in Fig. 4 are model calculations from the collisional-radiative code FLYCHK (see Ref. [20]). At $T_e = 150$ eV, FLYCHK predicts a slightly higher average ionization $\langle Z \rangle \simeq 16.5$. It is interesting to note that FLYCHK and GALAXY predict broader distributions than CLOUDY. For example, for T_e between 70 and 210 eV, GALAXY predicts an average charge that varies between 16.2 and 16.4 and a FWHM that varies between 1.6 and 1.7, much broader than 1.2 for CLOUDY. Differences in the widths are likely due to differences in the specific rates that couple the Fe^{15+}, Fe^{16+}, and Fe^{17+} ions. Understanding these differences between models, as well as including better atomic data where needed, such as R-matrix rates, is the subject of future work.

In this experiment we set out to produce a low density photoionized iron plasma in order to create conditions that would allow a meaningful comparison with x-ray emission from astrophysical sources. We believe that these are the first laboratory experiments in which the charge state distribution was measured in a well characterized, strongly photoionized plasma where the ionization parameter reached values of $\xi = 20$–25 erg cm s^{-1}, an ionization regime relevant to astrophysical x-ray sources. We hope these results will motivate further experiments at the ZR-facility upgrade and at the National Ignition Facility at LLNL, where even higher radiation fluxes are anticipated.

The authors thank T. R. Kallman, H. Netzer, G. J. Ferland, and R. W. Lee for helpful discussions, M. K. Matzen, A. L. Osterheld, and M. Eckart for their support, and J. Emig, D. L. Fehl, and the Sandia Z-facility team for their technical assistance. This work was performed under DOE UC Contract No. W-7405-Eng-48. P. v. H., S. J. R., and F. P. K. acknowledge support from the U.K. Engineering and Physical Sciences Research Council, the AWE Aldermaston William Penney Foundation, and NATO Grant No. CLG979443.

[1] F. Paerels *et al.*, Astrophys. J. **533**, L135 (2000).
[2] J. S. Kaastra *et al.*, Astron. Astrophys. **354**, L83 (2000).
[3] P. Beiersdorfer *et al.*, Astrophys. J. **519**, L185 (1999).
[4] D.W. Savin *et al.*, Astrophys. J. **489**, L115 (1997).
[5] K.B. Fournier *et al.*, in *Proceedings of the Workshop on Data Needs for X-Ray Astronomy*, edited by M. A. Bautista, T. R. Kallman, and A. K. Pradhan (Goddard Space Flight Center, Greenbelt, MD, 2000), p. 127.
[6] R. F. Heeter *et al.*, *Proceedings of the Workshop on Data Needs for X-Ray Astronomy* (Ref. [5]), p. 135.
[7] Y. Morita *et al.*, J. Quant. Spectrosc. Radiat. Transfer **71**, 519 (2001).
[8] R.F. Heeter *et al.*, Rev. Sci. Instrum. **72**, 1224 (2001).
[9] M. E. Foord *et al.*, in *Spectroscopic Challenges of Photoionized Plasmas*, edited by G. J. Ferland and D.W. Savin, ASP Conf. Series No. 247 (Astronomical Society of the Pacific, San Francisco, 2001), p. 117.
[10] J. E. Bailey *et al.*, Phys. Plasmas **9**, 2186 (2002).
[11] L. E. Ruggles *et al.*, Rev. Sci. Instrum. **72**, 1218 (2001).
[12] G. A. Chandler *et al.*, Rev. Sci. Instrum. **70**, 561 (1999).
[13] T.W. L. Sanford *et al.*, Rev. Sci. Instrum. **68**, 852 (1997).
[14] C. B. Tarter, W. H. Tucker, and E. E. Salpeter, Astrophys. J. **156**, 943 (1969).
[15] D. Mihalas, *Stellar Astrophysics* (Freeman and Co., San Francisco, 1978).
[16] L. Spitzer, *Physics of Fully Ionized Gases* (Interscience Publications, Inc., New York, 1956).
[17] M. Klapisch, J. L. Schwob, B. S. Fraenkel, and J. Oreg, J. Opt. Soc. Am. **67**, 148 (1977).
[18] R. L. Kelly, J. Phys. Chem. Ref. Data **16**, Suppl. No. 1, 860 (1987).
[19] S. J. Rose, J. Phys. B **31**, 2129 (1998).
[20] H.-K. Chung, W. L. Morgan, and R.W. Lee, J. Quant. Spectrosc. Radiat. Transfer **81**, 107 (2003).
[21] G. J. Ferland *et al.*, Publ. Astron. Soc. Pac. **110**, 761 (1998).